Vol 13 No 6, June 2004
1009-1963/2004/13(06)/0836-09

Chinese Physics

© 2004 Chin. Phys. Soc.
and IOP Publishing Ltd

Electromagnetic dissociation of 3.7 A GeV ^{16}O in nuclear emulsion*

Li Jun-Sheng(李俊生), Zhang Dong-Hai(张东海)†
Li Zhen-Yu(李振宇), and Wu Feng-Juan(吴凤娟)

Institute of Modern Physics, Shanxi Teachers' University, Linfen 041004, *China*

(Received 6 June 2003; revised manuscript received 18 December 2003)

The electromagnetic dissociation (ED) of 3.7 A GeV ^{16}O in nuclear emulsion is investigated with high statistics. It is found that the electromagnetically dissociated cross section increases with increasing beam energy, the charge distribution of projectile fragments is the same as the results at 60 and 200 A GeV, and the production probability of projectile fragments with charge $3 \leq Z \leq 5$ is less than that of the other projectile fragments. These results can be well explained by use of Weizsacker and Williams method for calculating the ED contributions. The percentile abundance of various decay modes for ED at 3.7 A GeV is close to the result at 60 and 200 A GeV, but it is different from the result at 14.6 A GeV. The ED of 3.7 A GeV is mainly caused by the giant dipole and quadrupole resonance of E1 and E2, which can be qualitatively explained by the multiplicity distribution of projectile proton in ED. The multiplicity distribution of the α fragments in ED and nuclear events have different functional forms. This difference may be a consequence of the different reaction mechanism involved.

Keywords: electromagnetic dissociation, projectile fragments, fragmentation
PACC: 2570N, 2520, 2587

1. Introduction

Since the availability of relativistic heavy ions from accelerator facilities at the CERN Super Proton Synchrotron (SPS) and BNL Alternating Gradient Synchrotron (AGS), considerable studies have been done in every aspect of relativistic nucleus–nucleus collisions. The main objective of the study of nucleus–nucleus collision at such energies is to observe the signatures of new forms of nuclear matter like quark–gluon plasma (QGP) at very small values of the impact parameter of collision (central collision). Peripheral collisions are used to study the fragmentation of spectators. However, in collisions involving impact parameters larger than the range of the nuclear force, extremely strong electromagnetic fields are produced for a short period of time. These varying electromagnetic fields have also led to an interesting domain of physics that has attracted more and more attention in relation to relativistic heavy ion collisions. The electromagnetically dissociated cross section increases with the increase of target mass and projectile energy, and will be greater than the nuclear cross section in BNL Relativistic Heavy Ion Collidor (RHIC) and the CERN Large Hardronic Collidor (LHC) energies, and is expected to dominate the interaction of highly charged objects at high energies.

For the heavier targets electromagnetic dissociation (ED) is expected to play an important role in the process of projectile fragmentation. ED occurs when a projectile nucleus which passes along a heavy target consisting of nuclei is excited by the Coulomb field of the target. In relativistic motion this field is equivalent to a violent electromagnetic pulse incident on the projectile. In a subsequent step the decay of the excited nucleus by emission of one or more nucleons is possible.

The first evidence for ED in relativistic heavy ion collisions was reported in a cosmic ray experiment by Balasubrahmanyan *et al*[1,2] for carbon and oxygen projectiles interacting with a tungsten target. Heckman and Lindstrom[3] analysed ED with heavy ion

*Project supported by the National Natural Science Foundation of China(Grant No 10275042), the Natural Science Foundation of Shanxi Province (Grant No 20021007) and Shanxi Provincial Foundation for Returned Scholars, China.
†E-mail: zhangdh@dns.sxtu.edu.cn

beams accelerated at the Lawrence Berkeley Laboratory (LBL) Bevalac for ^{16}O and ^{12}C projectiles at 2.1 A GeV colliding on Ag and Pb targets. With the availability of relativistic heavy ions from accelerator facilities at the CERN SPS and BNL AGS, systematic studies have been done for ED of projectiles and targets at the above energies, JINR Dubna and LBL Bevalac energies. For ED of projectiles in nuclear emulsion many works [4–14] have been performed in recent years. It is found that the total ED cross section increases with the increase of projectile energy, which can be well reported by a quantum mechanical approach to the virtual photon method using the plane wave Born approximation,[15] and the charge-changing cross section of the projectile from ED can be well explained by the Weizsacker and Williams method.[16–18]

2. Theory of electromagnetic dissociation

In the model of Weizsacker and Williams the electromagnetic field of a point-charge target is seen by a passing point-charge projectile as a flux of photons. The photon energy spectrum is calculated classically by the Fourier transform of the time-varying electromagnetic field,

$$\frac{\mathrm{d}I}{\mathrm{d}W} = \frac{2Z_{\mathrm{T}}^2 e^2}{\pi c\beta^2}\left\{ xk_0(x)k_1(x) - \frac{1}{2}\beta^2 x^2[k_1^2(x) - k_0^2(x)]\right\}, \qquad (1)$$

where k_i are modified Bessel functions of order i, and $x = \omega b/\beta\gamma c$. Here b is the impact parameter, γ the Lorentz factor, and β the velocity of the incident charge in units of c. Putting the photon energy $E_\gamma = h\omega$, the maximum energy of the spectrum is $E_{\gamma\max} \approx h\gamma c/b_{\min}$, where $b_{\min}$, the minimum impact parameter, is in practice the sum of the radii of the colliding nuclei. At Dubna energies (3.7 A GeV), $E_{\gamma\max} \approx 85$ MeV; whereas at AGS energies (14.5 A GeV), $E_{\gamma\max} \approx 320$ MeV, and at CERN energies (200 A GeV), $E_{\gamma\max} \approx 4500$ MeV. The number of photon quanta $N(E_\gamma)$ per unit area at an energy as seen by a moving projectile from the stationary target is given by

$$N(E_\gamma) = \frac{2\alpha Z_{\mathrm{T}}^2}{\pi E_\gamma \beta^2}\left\{ xk_0(x)k_1(x) - \frac{1}{2}\beta^2 x^2[k_1^2(x) - k_0^2(x)]\right\}, \qquad (2)$$

where α is the fine structure constant.

For $E_\gamma \ll E_{\gamma\max}$ (in practice, for $E_\gamma < 0.2E_{\gamma\max}$) and $\beta \approx 1$, Eq.(2) can be approximately written as

$$N(E_\gamma) = \frac{2\alpha Z_{\mathrm{T}}^2}{\pi E_\gamma}\left[\ln(1.123\hbar\gamma c/E_\gamma b_{\min} - \frac{1}{2}\right]. \qquad (3)$$

It must be noted that nuclear emulsion is a heterogeneous target but, owing to the Z_{T}^2 dependence in Eq.(3), the heaviest constituents (Ag and Br) contribute more than 95% of the total intensity. Figure 1 shows the low-energy part of the photon spectrum for ^{16}O projectile at 3.7 A GeV for the various constituents of the nuclear emulsion.

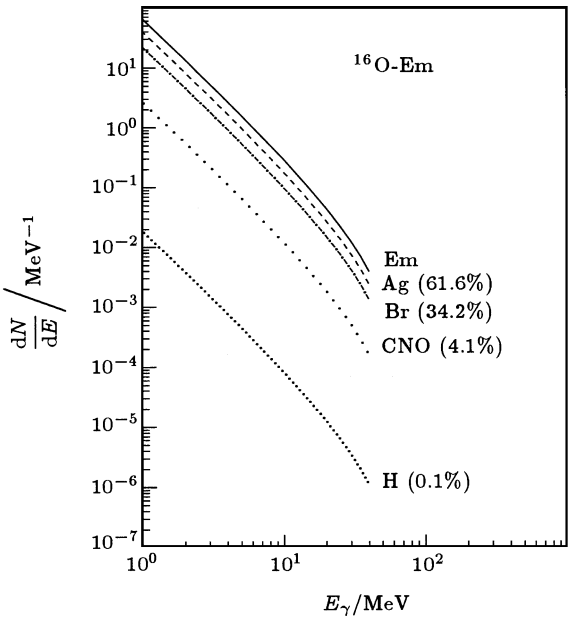


Fig.1. The energy spectra of virtual photons for ^{16}O projectile on emulsion nuclei at 3.7 A GeV.

3. Experimental details

In the present investigation an emulsion stack provided by EMU-01 Collaboration comprising of 30 plates of NIKFI BR-2 emulsion, each of dimensions $10 \times 10 \times 0.06\,\mathrm{cm}^3$ and exposed horizontally to 3.7 A GeV ^{16}O beam at JINR Dubna, has been used. The beam flux intensity was 10^3particles/cm^2. In order to obtain an unbiased sample of events, an along-track scanning technique was adopted. The pellicles were scanned under 100× magnification, using oil immersion objectives in SXJ-1 and SXJ-2 microscopes. The tracks were picked up at a distance of 1 cm from the edge of the pellicles and were carefully followed until they either interacted with the nuclei of the emulsion or escaped from the pellicle. If an interaction

occurred, the following characteristic features were recorded: N_b, the number of black tracks (mostly protons of energies $E \leq 26$ MeV); N_g, the number of grey tracks (recoil protons in the kinetic energy range $26 \leq E \leq 375$ MeV and a few kaons of kinetic energies $20 \leq E \leq 198$ MeV and pions with kinetic energies of $12 \leq E \leq 56$ MeV); N_s, the number of minimum ionizing shower tracks (mostly pions with velocity $\beta \geq 0.7$); N_f, the number of projectile fragments (PFs) of charge $Z \geq 2$.

The charges of all the PFs($Z \geq 2$) were determined by measurement of grain density and by counting the δ-rays in a fixed track length. Specifically, the method of grain density was applied to discriminate charge $Z = 2$. On the other hand, for PFs in the charges $3 \leq Z \leq 8$, the method of δ-rays counting was used to measure the charge of PFs. For determining the charge of PFs with charges $3 \leq Z \leq 8$, the following relation was used:

$$\frac{N_\delta(Z)}{Z^2} = \frac{N_\delta(^{16}\mathrm{O})}{8^2}, \tag{4}$$

where $N_\delta(Z)$ and $N_\delta(^{16}\mathrm{O})$ is the number of δ-rays of PFs with charge Z and ^{16}O beam per 100 μm track length, respectively. The accuracy of the Z determination was always better than ± 1 unit. Here, we obtained the δ-ray per 100μm distribution (Fig.2) for PFs having charges $3 \leq Z \leq 7$ emitted from a ^{16}O projectile by following each track for at least 1mm track length. Each of these histograms can be fitted by a Gaussian distribution with a peak corresponding to a certain value of Z.

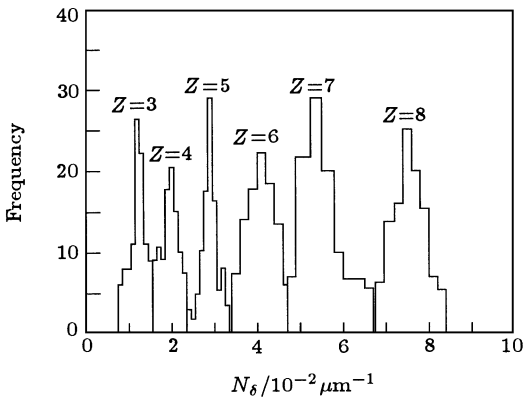


Fig.2. The frequency distribution of PFs as a function of N_δ per 100 μm.

Each event was qualitatively classified into two principal categories depending upon visual characteristics.

1) Nuclear events. Nuclear events may be central or peripheral. Central events are the events which exhibit no PFs with $Z \geq 2$ in the forward cone. Such events are thought to be produced by violent destruction of the projectile and target nuclei at small values of impact parameter b of collision. Peripheral events are the events with PFs of charge $Z \geq 2$ emitted in a forward cone; these events show considerably less involvement of the projectile nucleus since they are formed at relatively large values of b.

2) Electromagnetic events. Events generated by the ED of the projectile nucleus are produced in collisions involving impact parameters large enough so that no nuclear interactions occur. Extremely strong electromagnetic fields from the heavy nuclei are produced for a very short time at the projectile. Such events typically consist of PFs which proceed in the direction of motion of the projectile nucleus and are confined within 45 mrad to the beam direction.

We followed a total track length of 28390.4 cm, during which 2292 events were observed, giving rise to a total interaction mean free path $\lambda = 12.39 \pm 0.26$ cm. In this analysis it is very important to distinguish peripheral events from ED, since the former class of events may, in some cases, exhibit topologies similar to the latter. Confusion may arise in grazing collisions, where a few pion tracks are produced in addition to the projectile protons. To achieve this necessary distinction, we impose a limit on the fragmentation cone for PFs. The fragmentation cone is defined by $\Theta \leq \Theta_c = p_f/p_{beam}$, where p_{beam} stands for the beam momentum and p_f for the Fermi momentum; the latter is estimated to be ≈ 200 MeV/c for the ^{16}O ions at 3.7 A GeV, thus giving $\Theta_c \approx 45$ mrad. The value of Θ_c was chosen such that the probability of finding the produced shower particles among the projectile fragments (in grazing collisions) in the fragmentation cone is very low. The EDs were then picked up using the criterion that the total charge of the PFs ($Z \geq 1$) inside this cone is 8.

In order to eliminate events produced by elastic collisions, events with a single black or grey track emerging from the undeviated beam track were not considered. To avoid inclusion of fast δ-rays and low energy e^+e^- pairs sitting on the beam tracks, the events with a single shower track were re-examined. If the shower track under consideration received significant effects of Coulomb scattering when followed for at least 3 cm, the event was not included in our sample. Considering all the above conditions, the

EDs must satisfy the following criteria: (1) $n_b = 0$ and $n_g = 0$; (2) the total charge of PFs ($Z \geq 1$) inside the fragmentation cone is equal to 8; (3) there are no shower particles n_s outside Θ_c. After applying the above stringent selection criteria, 111 events were found to be produced by electromagnetic interactions and 109 events were due to elastic interactions, out of a total 2292 observed events.

4. Experimental results

4.1. The charge spectra

In Fig.3(a), we show the charge spectrum of all the PFs ranging from $Z = 1$ to Z=7 emitted in the ^{16}O beams at 3.7 A GeV. For comparison, the results at 14.6, 60 and 200 A GeV [7,14] are also presented in the figure. At the three energies 3.7, 60 and 200 A GeV, the charge distribution of projectile fragments have the same tendency: the most abundant PF is with $Z = 1$, the next one is with $Z = 2$; the least abundant are the PFs with charges in the range of $3 \leq Z \leq 5$; PF with charge $Z = 7$ has the relative yield almost two times higher than that of $Z = 6$, but these are different from the results at 14.6 A GeV. Figure 3(b) exhibits the charge spectra of all PFs ranging from $Z = 1$ to $Z = Z_p - 1$ for ED events of ^{16}O, ^{24}Mg, ^{28}Si and ^{32}S at the same energy 3.7 A GeV,[11,12] where Z_p is the charge of the projectile. From this figure, one can conclude that

(1) the most abundant PF is with charge $Z = 1$ and next one is with $Z = 2$;

(2) the least abundant are the PFs with charges in the range of $3 \leq Z \leq 5$ for all beams;

(3) for heavier beams there is a slow increase in the relative abundance of charges between $6 \leq Z \leq 11$;

(4) PF with charge $Z = Z_p - 1$ has a relative yield almost two times that of PF with charge $Z = Z_p - 2$ for all projectiles.

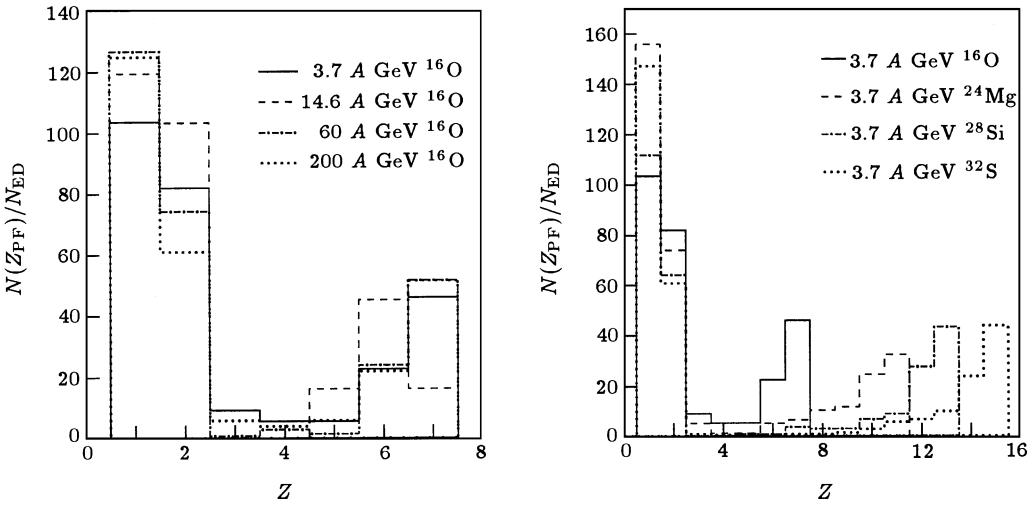


Fig.3. The multiplicity distributions of projectile fragments with charge $1 \leq Z \leq Z_p - 1$ for ED events emerging from (a) ^{16}O at 3.7, 14.6, 60 and 200 A GeV, (b) ^{16}O, ^{24}Mg, ^{28}Si and ^{32}S at the same energy 3.7 A GeV.

4.2. Mean free paths of nucleus (λ_{nuc}) and ED (λ_{ED})

In Table 1, we present the topologies of the inelastic and electromagnetic interactions observed. We also include here the results from Refs.[7–14] on different types of interactions. Table 1 indicates that ED as a percentage of the nuclear events (N_{nuc}) increases with the total projectile energy: that is, the value of electromagnetic dissociated cross section (λ_{ED}) increases (decreases) with the increase of the total projectile energy. For the same projectile ^{16}O, the value of λ_{ED} decreases with the increase of projectile energy. These observations are in qualitative agreement with the predictions of the virtual photon theory.[15,16]

Table 1. The data of the number of primary nuclear($N_{\rm nuc}$) and electromagnetic dissociated ($N_{\rm ED}$) interactions of different ions in the nuclear emulsion.

Ion	Energy/A GeV	Scanned length/m	$N_{\rm nuc}$	$N_{\rm ED}$	$\lambda_{\rm nuc}$/cm	$\lambda_{\rm ED}$/cm	ED as % of $N_{\rm nuc}$	Ref.
^{7}Li	3.0	147.44	970	45	15.20 ± 0.50	327.64 ± 49.60	4.64	[13]
^{6}Li	3.7	140.36	968	70	14.50 ± 0.50	200.51 ± 40.44	7.23	[13]
^{12}C	3.7	144.00	1000	60	14.40 ± 0.33	236.00 ± 28.20	6.00	[13]
^{16}O	3.7	86.23	708	81	12.18 ± 0.33	106.45 ± 10.68	11.43	[13]
^{16}O	3.7	283.90	2072	111	13.70 ± 0.30	255.77 ± 24.28	5.36	This paper
^{24}Mg	3.7	98.50	1025	77	9.61 ± 0.30	127.92 ± 14.58	7.51	[11]
^{28}Si	3.7	35.93	400	25	8.98 ± 0.45	143.72 ± 28.74	6.25	[11]
^{16}O	14.6	67.24	501	31	13.42 ± 0.60	216.90 ± 38.96	6.19	[9]
^{28}Si	14.5	174.89	1408	109	12.42 ± 0.33	160.45 ± 15.37	7.74	[7]
^{28}Si	14.6	71.69	691	46	10.37 ± 0.39	155.85 ± 22.98	6.66	[9]
^{16}O	60	16.37	131	9	12.50 ± 1.09	181.89 ± 60.63	6.87	[10]
^{16}O	60	220.98	1691	151	13.07 ± 0.32	146.34 ± 11.91	8.93	[14]
^{16}O	200	117.19	957	113	12.25 ± 0.40	103.71 ± 9.76	11.81	[7]
^{16}O	200	69.31	591	68	11.73 ± 0.48	101.91 ± 12.36	11.51	[9]
^{16}O	200	348.70	2934	362	11.88 ± 0.22	96.33 ± 5.10	12.34	[8]
^{32}S	200	198.50	2168	476	9.15 ± 0.20	41.70 ± 1.91	21.96	[8]

4.3. Observed modes of decay in ED

In Table 2, we present a summary of the identified events in ^{16}O–Em interaction. Results taken from Refs.[7–9,14] are also included to facilitate the comparison. In the first column of Table 2, the decay mode of an observed channel, deduced from the charge conservation, is given. It should be noted that, in this experiment, only the charge of each PF is determined. The mass of the fragment is speculative and stable isotopes of heavy fragments may as well be produced. Since neutron cannot be detected in the emulsion, the disintegration mode ^{15}O+n, expected to be similar to the ^{15}N+p mode, has escaped detection. Furthermore, the mode ^{14}N+p,n cannot be distinguished from the ^{15}N+p mode, and so on. The second column shows the threshold energy ($\triangle E_{\rm th}$) for the excitation of a given mode calculated in the rest of the projectiles by using the mass defect formula. The third column indicates the number of ED events ($N_{\rm ED}$) observed in each mode. The fourth column gives the relative rates for the various visible modes. The relative rates for the various visible modes at 3.7 A GeV, within statistical error, are close to the results at 60 A GeV,[14] and 200 A GeV,[7–9] but are different from the results at 14.6 A GeV.[9] Table 2 indicates that the major decay mode of ED at 3.7, 60 and 200 A GeV is ^{16}O$\rightarrow^{15}$N+p, and then the modes ^{16}O$\rightarrow^{12}$C+α and ^{16}O$\rightarrow^{12}$C+2D; the relative rates of the former modes is almost two times the latter. Figure 4 shows the relative rate (per 30 MeV) of different decay modes as a function of the threshold energy in ED events from ^{16}O beams. Data obtained at 14.6 A GeV[9], 60 A GeV[14] and 200 A GeV[7–9] are also included in this figure. These data can be approximately represented by the relation $Y = \exp(k_1 \triangle E_{\rm th} + k_2)$. Using a minimum χ^2 fit we obtain $k_1 = -0.047\,{\rm MeV}^{-1}$, $k_2 = 0.43$ (minimum $\chi^2 = 3.507$) for the data at 3.7 A GeV; $k_1 = -0.044\,{\rm MeV}^{-1}$, $k_2 = 0.33$ (minimum $\chi^2 = 1.053$) for the data at 60 A GeV; $k_1 = -0.043\,{\rm MeV}^{-1}$, $k_2 = 0.31$ (minimum $\chi^2 = 0.861$) for data at 14.6 A GeV; and $k_1 = -0.041\,{\rm MeV}^{-1}$, $k_2 = 0.262$ (minimum $\chi^2 = 11.42$) for the data at 200 A GeV. From these simulation results we obtain that the parameter k_1 increases with the increase of projectile energy, and the parameter k_2 decreases with the projectile energy.

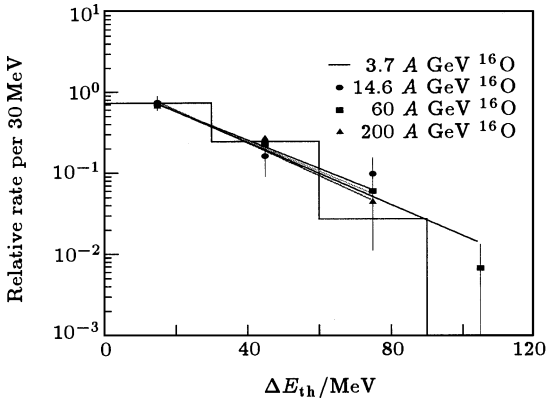


Fig.4. Variation of the relative rate per 30 MeV with the threshold energy $\triangle E_{\rm th}$ for various decay modes observed in ^{16}O ED collisions at different energies.

Table 2. Threshold energy($\triangle E_{\rm th}$), observed number of EDs and ED fraction presented in different decay modes for ^{16}O at 3.7, 14.6, 60 and 200 A GeV.

Decay mode	$\triangle E_{\rm th}$	3.7 A GeV		60 A GeV		14.6 A GeV		200 A GeV	
		$N_{\rm ED}$	Fraction(%)	$N_{\rm ED}$	Fraction(%)	$N_{\rm ED}$	Fraction(%)	$N_{\rm ED}$	Fraction(%)
^{15}N+p	12.1	51	45.95 ± 6.43	78	51.66 ± 5.85	5	16.13 ± 7.21	281	53.12 ± 3.17
^{12}C+α	7.2	15	22.52 ± 4.50	20	23.84 ± 3.97	12	45.16 ± 12.07	52	24.20 ± 2.14
^{12}C+2D	31.0	10		16		2		76	
^{11}B+α+p	23.1	3	10.81 ± 3.12	2	3.97 ± 1.62	5	16.13 ± 7.21	25	9.83 ± 1.36
^{11}B+2D+p	47.0	1						3	
^{10}B+^{6}Li	30.9	2							
^{8}Be+α+2D	38.4	3		2				11	
^{8}Be+2α	14.6	3							
^{8}Be+^{7}Li+p	31.9							9	
^{8}Be+4D	62.2			2				4	
^{7}Li+2α+p	31.8	4	6.31 ± 2.38	1	0.66 ± 0.66		3.23 ± 2.24	6	3.02 ± 0.76
^{7}Li+α+2D+p	55.6					1		5	
^{7}Li+4D+p	79.5	2						5	
2^{7}Li+2p	49.1	1							
4α	14.4	9	14.41 ± 3.60	7	19.21 ± 3.57	1	19.35 ± 7.90	10	9.83 ± 1.36
3α+2D	38.3	6		15		2		22	
2α+4D	62.1	1		6		1		16	
α+6D	86.0			1		2		4	
8D	109.8			1					

4.4. Cross sections $\sigma_{\rm nuc}$ and $\sigma_{\rm ED}$

4.4.1. Nuclear interaction cross section $\sigma_{\rm nuc}$

The nuclear interaction cross section can be calculated experimentally from the relation

$$\sigma_{\rm nuc} = f/\rho\lambda_{\rm nuc}, \qquad (5)$$

where $\rho = 8.133 \times 10^{22}$ atoms per cm^3 is for NIKFI BR-2 emulsion and f is a weight factor which is unity for nuclear interactions produced by all the emulsion targets. In Table 3, we present our experimental data along with the data by other investigators of the production cross sections for nuclear and electromagnetic events.[7−11,14] Table 3 indicates that the nuclear cross sections of ^{16}O, within experimental errors, are the same at four different energies. In order to compare the experimentally obtained value of $\sigma_{\rm nuc}$ with the theoretical prediction, we have used the semi-empirical expression of $\sigma_{\rm nuc}$ given by Westfall *et al.*[19]

$$\sigma_{\rm nuc}^{\rm th} = \pi[r_0(A_{\rm P}^{1/3} + A_{\rm T}^{1/3} - b)]^2, \qquad (6)$$

where r_0 = 1.35 fm and b=0.83. Since this formula is valid for $A_{\rm P} \geq 12$ and $A_{\rm T} \geq 12$, we used $A_{\rm T}$=48.39 for standard nuclear emulsion after neglecting the contribution from the ^{1}H target, and obtained $\sigma_{\rm nuc}$=1628 mb (for NIKFI BR-2 emulsion $A_{\rm T}$=47.46, $\sigma_{\rm nuc}$=1614 mb) with $A_{\rm P}$=16. The corresponding experimental value of $\sigma_{\rm nuc}$, after excluding the contribution of the ^{1}H target, is found to be 1634 ± 40 mb (1541 ± 38 mb for NIKFI BR-2 emulsion), showing that these values are in close agreement with one another. Considering the contribution from the ^{1}H targets, formula (6) cannot give a reasonable value of $\sigma_{\rm nuc}$(^{16}O, ^{1}H). As discussed in Ref.[20] for the validity of the usage of expression (6) for hydrogen target, we have chosen $A_{\rm T}$=0.089. Using this value of $A_{\rm T}$ for hydrogen target and other values for heavier targets of nuclear emulsion, in conjunction with their number densities, the theoretical value of nuclear cross section $\sigma_{\rm nuc}$ is 1152 mb for ^{16}O projectile in the standard nuclear emulsion. The calculated value of $\sigma_{\rm nuc}$ for ^{16}O at 200 A GeV agrees quite well with those of measured ones within experimental errors, but is larger than the measured ones at 3.7, 14.6 and 60 A GeV (Table 3).

Table 3. Nuclear cross sections $\sigma_{\rm nuc}$ for all targets of emulsion and ED cross section $\sigma_{\rm ED}$ for the Ag target only. The weight factor f is explained in the text.

Beam	Energy/A GeV	$\sigma_{\rm nuc}^{\rm exp}$/mb	$\sigma_{\rm nuc}^{\rm th}$/mb	f	$\sigma_{\rm ED}$/mb	Ref.
^{16}O	3.7	897 ± 20	1152	0.61	230 ± 22	This paper
^{24}Mg	3.7	1335 ± 42	1342	0.62	475 ± 55	[11]
^{28}Si	3.7	1428 ± 72	1436	0.62	423 ± 88	[11]
^{28}Si	14.5	1019 ± 27	1436	0.62	383 ± 37	[7]
^{28}Si	14.5	1221 ± 46	1436	0.62	394 ± 58	[9]
^{16}O	14.6	943 ± 42	1152	0.62	283 ± 51	[9]
^{16}O	60	941 ± 42	1152	0.61	402 ± 33	[14]
^{16}O	60	1013 ± 88	1152	0.62	337 ± 112	[10]
^{16}O	200	1033 ± 38	1152	0.62	592 ± 57	[7]
^{16}O	200	1079 ± 44	1152	0.62	602 ± 73	[9]
^{16}O	200	1066 ± 20	1152	0.61	670 ± 35	[8]
^{32}S	200	1384 ± 30	1427	0.61	1680 ± 80	[8]

4.4.2. Electromagnetic dissociated cross section $\sigma_{\rm ED}$

In order to obtain the absolute value of the cross section for ED and also to compare the present results with those of other experiments, we converted the observed mean free path in the emulsion into absolute cross section of Ag target (the heaviest and most abundant element in the emulsion). The contribution of the elements such as iodine and sulfur, whose abundance in the nuclear emulsion are very small, is neglected. The total production cross section for ED events on the Ag target is then computed from the relation

$$\sigma_{\rm ED} = f/\rho\lambda_{\rm ED}, \tag{7}$$

where $\rho = 1.01 \times 10^{22}$ atoms per cm^3 is the density of Ag in standard nuclear emulsion (for NIKFI BR-2 emulsion which is 1.04×10^{22} atoms per cm^3). The factor f is an appropriate weight obtained for Ag targets from the following equation:

$$f = \frac{N_{\rm T} Z_{\rm T}^2}{\sum_i N_i Z_i^2}, \tag{8}$$

where $N_{\rm T}$ is the number of Ag atoms/ml and $Z_{\rm T} = 47$ is its nuclear charge. The denominator represents a summation over all the targets (namely Ag, Br, C, N, O, and H) of the nuclear emulsion. The value of f obtained in the present work is 0.61. The values of $\sigma_{\rm ED}$, thus obtained, are given in Table 3, which indicates that the ED cross sections increase with the projectile energy for the same projectile (as shown in Fig.5).

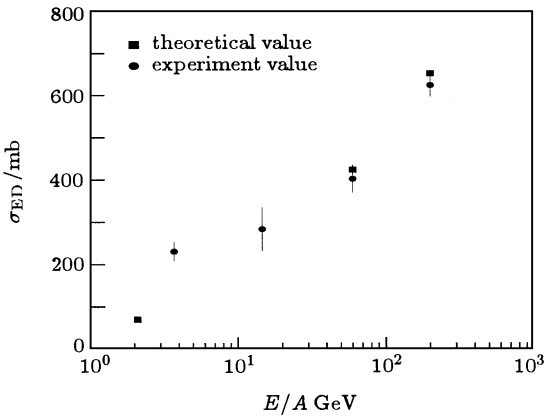


Fig.5. ED cross section of ^{16}O on ^{108}Ag target as a function of the projectile energy.

4.5. The multiplicity distribution of projectile fragments produced in ED for ^{16}O in the emulsion

4.5.1. The multiplicity distribution of projectile proton

The investigation of multiplicity distribution of projectile fragments produced in ED events is quite important in understanding the reaction mechanism involved. In Fig.6 we present the multiplicity distribution of projectile proton produced in ED interaction at 3.7 A GeV; the results at 14.6 A GeV,[9] 60 A GeV [14] and 200 A GeV ^{16}O [7,9] are also included. The multiplicity distribution at 3.7 A GeV is different from the ones at 60 and 200 A GeV. For the multiplicity distribution at 3.7 A GeV, only one peak exists at $N_{\rm p} = 1$, but for the distribution at 60 and 200 A GeV there are two peaks which can be well reproduced by two Gaussian distributions. At 3.7 A GeV energy the peak is at $N_{\rm p} = 1$ which is the same as

the first peak at 60 and 200 A GeV, corresponding to $\triangle E_{\rm th} \leq 30$ MeV. In this region the giant dipole and the quadrupole resonance is excited by E1 and E2 photons, and the major decay channels of projectile fragmentation are ^{16}O$\rightarrow^{12}$C+$\alpha(\triangle E_{\rm th}$=7.2 MeV), ^{16}O$\rightarrow^{15}$N+p$(\triangle E_{\rm th}$=12.1 MeV), and ^{16}O$\rightarrow 4\alpha(\triangle E_{\rm th}$= 14.4 MeV). The peak of second Gaussian distribution at 60 and 200 A GeV is at $N_{\rm p}$=4, corresponding to $\triangle E_{\rm th}$=63 MeV. In this region the maximum threshold to EDs is 110 MeV, which mainly comes from the quasi-deuteron effect.

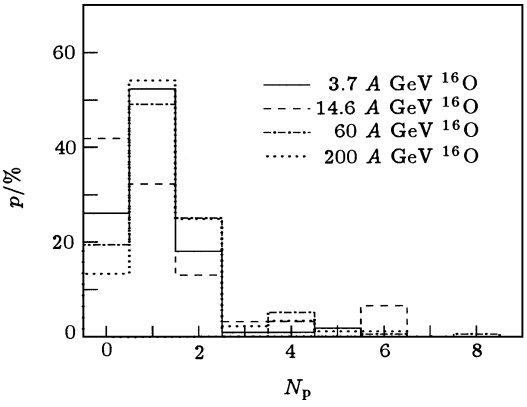


Fig.6. The multiplicity distributions of the projectile proton produced in ED at different energies.

4.5.2. Multiplicity distribution of α fragments

Finally, we study the multiplicity distribution of α projectile fragments produced in ED interactions. There are a number of studies which have been performed for the multiplicity distribution of α projectile fragments produced in nuclear interactions,[21−26] and it can be concluded that the multiplicity distribution of α projectile fragments obeys a scaling law predicted by Koba, Nielsen, and Olesen:[27]

$$\psi(Z) = < n_\alpha > p(n_\alpha) = < n_\alpha > \sigma_{n\alpha}/\sigma_{\rm nuc}. \quad (9)$$

This is an energy-independent function of the scaled variable $Z = n_\alpha / < n_\alpha >$, where n_α represents the number of α particles produced in an event and $< n_\alpha >$ is the average multiplicity of α particle of the whole data samples. The multiplicity distribution of α particle produced in nuclear interactions can be reproduced by a universal function $\psi(Z) = AZe^{-BZ}$, where A and B are constants whose values can be determined experimentally. In Fig.7, we plot $< n_\alpha > p(n_\alpha)$ as a function of the scaled variable $n_\alpha / < n_\alpha >$ for α fragments produced in ED events at 3.7 A GeV. The results at 14.6,[9] 60 [14] and 200 A GeV [7,9] are also included in the figure. The following functional form has been fitted through the data points: $\Phi(Z) = aZ^b$, where $a = 0.17$ and $b = -0.93$ with χ^2/d.o.f.=0.49, which is coincident with the results at 60 A GeV(a = 0.24 and $b = -1.33$ with χ^2/d.o.f.=0.02) and 200 A GeV($a = 0.28$, $b = -1.24$ with χ^2/d.o.f.=0.02), where d.o.f. means degree of freedom. The fact that the two different functional forms must be fitted through the data points for ED events and nuclear events, may be a consequence of their different reaction mechanisms involved.

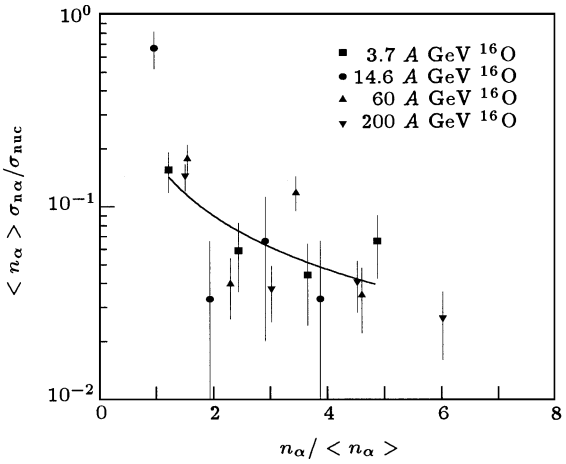


Fig.7. The multiplicity distribution of α projectile fragments emitted in the ED of ^{16}O with different energies in the emulsion.

5. Conclusions

In this paper, we have investigated the ED of 3.7 A GeV ^{16}O ions from the JINR Dubna. The results are compared with the available data on electromagnetic interactions in the emulsion. The following summarizes the important conclusions of this work.

1) The absolute value of the overall charge-changing cross section($\sigma_{\rm ED}$) for the Ag target increases with the projectile energy. The charge distribution of the projectile fragments at 3.7 A GeV has the same tendency as at 60 and 200 A GeV.

2) The relative rates for the various visible decay modes at 3.7 A GeV, within the statistical errors, are close to the results of 60 and 200 A GeV, but are different from the results at 14.6 A GeV.

3) The majority of ED events at 3.7 A GeV may be attributed to the absorption of giant dipole and quadrupole resonance.

4) The multiplicity distributions of α fragments in ED events and nuclear events follow different functional forms. This difference may be a consequence of different reaction mechanisms involved in ED and nuclear events.

Acknowledgment

We are grateful to Professor I. Otterlund at Lund University in Sweden for supplying the emulsion plates.

References

[1] Balasubrahmanyan V K, Crannell C J, Hagen F A *et al* 1972 *Proc. 12th Int. Cosmic Ray Conf.* (Hobart, Tasmania)
[2] Artru X and Yodh G B 1972 *Phys. Lett.* B **40** 43
[3] Heckman H H and Lindstrom P J 1976 *Phys. Rev. Lett.* **37** 56
[4] Ahrens J, Borchert H, Czock K H *et al* 1975 *Nucl. Phys.* A **251** 479
[5] Vlasenko V G, Golgstein V A, Mitrofanova A V *et al* 1976 *Sov. J. Nucl. Phys.* **23** 265
[6] Singh G, Sengupta K and Jain P L 1990 *Phys. Rev.* C **41** 999
[7] Singh G and Jain P L 1992 *Z. Phys.* A **344** 73
[8] Baroni G, Bisi V, Breslin A C *et al* 1990 *Nucl. Phys.* A **516** 673
[9] Bahk S Y, Chang S D and Cheon B G 1991 *Phys. Rev.* C **43** 1410
[10] Ardito N, Baroni G, Bisi V *et al* 1988 *Europhys. Lett.* **6** 131
[11] Jilany M A 2002 *Nucl. Phys.* A **705** 477
[12] El-Nadi M, Abdelsalam A, Hussien A *et al* 2002 *J. Phys. G* **28** 241
[13] Yasin M N, Sherif M M, Abdelhalim S M *et al* 1997 *Sov. Phys. JETP* **84** 635
[14] Zhang D H and Sun H C 2001 *Acta Phys. Sin.* **49** 1938 (in Chinese)
[15] Bertulani C A and Baur G 1985 *Nucl. Phys.* A **442** 739
[16] Jackson J D 1975 *Classical Electrodynamics* (New York: Wiley)
[17] Von Weizsacker C F 1934 *Z. Phys.* **88** 612
[18] Williams E J 1934 *Phys. Rev.* **45** 729
[19] Westfall G D, Wilson L W, Lindstrom P J *et al* 1979 *Phys. Rev.* C **19** 1309
[20] Price P B, Ren G X and Williams W T 1988 *Phys. Rev. Lett.* **61** 2193
[21] Jain P L and Aggarwal M M 1986 *Phys. Rev.* C **33** 1790
[22] Singh G, Ismai A Z M and Jain P L 1991 *Phys. Rev.* C **43** 2417
[23] Sengupta K, Singh G and Jain P L 1989 *Phys. Lett.* B **222** 301
[24] Singh G and Jain P L 1994 *Z. Phys.* A **348** 99
[25] Admovich M A, Aggarwal M M, Arora R *et al* 1989 *Phys. Rev.* C **40** 66
[26] Admovich M A, Aggarwal M M, Alexandrov Y A *et al* 1994 *Phys. Lett.* B **338** 397
[27] Koba Z, Nielson B and Olesen P 1972 *Nucl. Phys.* B **40** 317